Acta Pharmaceutica Sinica B 2025;15(6):3008−3024

Chinese Pharmaceutical Association
Institute of Materia Medica, Chinese Academy of Medical Sciences

Acta Pharmaceutica Sinica B

www.elsevier.com/locate/apsb
www.sciencedirect.com

TOOLS

Phenotypic screening uncovered anti-myocardial fibrosis candidates using a novel 3D myocardial tissue under hypoxia

Jingyu Wang[a,†], Xiangning Liu[a,†], Rongxin Zhu[a], Ying Sun[a], Boyang Jiao[a], Keyan Wang[a], Yong Jiang[b], Yong Wang[c,d,e,*], Chun Li[d,f,g,*], Wei Wang[d,g,*]

[a]*School of Traditional Chinese Medicine, Beijing University of Chinese Medicine, Beijing 100029, China*
[b]*State Key Laboratory of Natural and Biomimetic Drugs, School of Pharmaceutical Sciences, Peking University, Beijing 100191, China*
[c]*Dongzhimen Hospital, Beijing University of Chinese Medicine, Beijing 100029, China*
[d]*Key Laboratory of Traditional Chinese Medicine Syndrome and Formula, Ministry of Education, Beijing 100029, China*
[e]*Yunnan University of Chinese Medicine, Kunming 650500, China*
[f]*Modern Research Center for Traditional Chinese Medicine, Beijing University of Chinese Medicine, Beijing 100029, China*
[g]*State Key Laboratory of Traditional Chinese Medicine Syndrome, Guangzhou University of Chinese Medicine, Guangzhou 510006, China*

Received 20 July 2024; received in revised form 17 August 2024; accepted 20 December 2024

KEY WORDS

Myocardial fibrosis;
3D myocardial tissue;
Toxicodendron vernicifluum;
Hypoxia;
Drug screening;
Primary cell;
Tissue contraction;
Hydrogel

Abstract Myocardial fibrosis (MF) is a common pathological hallmark of cardiovascular diseases, reflecting shared mechanisms in their progression. However, the lack of reliable MF models that accurately mimic its pathogenesis has hindered drug discovery, highlighting the urgent need for more effective therapeutic agents. Herein, a novel contractile three-dimensional (3D) myocardial tissue model integrating cardiomyocytes, cardiac-fibroblasts, and bone marrow-derived macrophages in collagen hydrogel was developed to simulate the fibrotic changes of cardiovascular disease, and facilitate the screening of anti-MF compounds. The 3D myocardial tissue model exhibited precise, visualizable, and quantifiable contractile characteristics under hypoxia and drug interventions. 76 compounds extracted from the resins of *Toxicodendron vernicifluum*, a traditional Chinese medicine with clear clinical benefits for fibrotic diseases, were screened for anti-fibrotic activity. Using

*Corresponding authors.
E-mail addresses: wangyong@bucm.edu.cn (Yong Wang), lichun19850204@163.com (Chun Li), wangwei26960@126.com (Wei Wang).
[†]These authors made equal contributions to this work.
Peer review under the responsibility of Chinese Pharmaceutical Association and Institute of Materia Medica, Chinese Academy of Medical Sciences.

https://doi.org/10.1016/j.apsb.2025.04.025
2211-3835 © 2025 The Authors. Published by Elsevier B.V. on behalf of Chinese Pharmaceutical Association and Institute of Materia Medica, Chinese Academy of Medical Sciences. This is an open access article under the CC BY-NC-ND license (http://creativecommons.org/licenses/by-nc-nd/4.0/).

an *in vitro* 3D oxygen−glucose deprivation (OGD)-treated myocardial tissue model instead of a two-dimensional transforming growth factor-β treated cardiac-fibroblasts model, two candidates including LQ-40 and SQ-3 exert impressive anti-MF activity, which was further validated in left anterior descending coronary artery ligation-induced MF mouse model. The current results demonstrate the feasibility and advantage of the novel contractile 3D tissue model with multi-cell types in discovering candidates for MF, further stressing the great potential of regulating macrophages in the treatment of MF.

© 2025 The Authors. Published by Elsevier B.V. on behalf of Chinese Pharmaceutical Association and Institute of Materia Medica, Chinese Academy of Medical Sciences. This is an open access article under the CC BY-NC-ND license (http://creativecommons.org/licenses/by-nc-nd/4.0/).

1. Introduction

Persistent excessive myocardial fibrosis (MF) represents the final pathological stage of cardiovascular diseases, posing an increasing threat to global health[1]. MF is defined by anomalous fibroblast proliferation and elevated extracellular matrix deposition, which leads to increased rigidity and diastolic dysfunction. This, in turn, results in functional cardiomyocyte (CMs) death, macrophage infiltration, and heart failure[2]. Current treatments for MF involve enhancing myocardial relaxation, oxygen utilization, and microcirculation while decreasing the release of cytokines linked to fibrosis in the microenvironment. Nevertheless, no ideal drugs are currently available for MF, accentuating the urgency for new efficient therapies that can prevent or improve MF[3].

The absence of predictive MF pathogenic models poses significant challenges in developing anti-MF treatments[4,5]. Currently, two-dimensional (2D) CFs (involving only one cell type of cardiac fibroblast) cultures with specific stimulation, such as transforming growth factor-β (TGF-β), are commonly used as *in vitro* MF models[6,7]. However, the 2D culture of CFs is limited in its ability to resemble the process of fibrosis development due to the lack of cell−matrix interactions and crosstalk with other essential cell types, including CMs and macrophages. As a result, 2D models often yield high false-positive or false-negative rates, leading to inefficient drug screening. Engineering three-dimensional (3D) cultures using different cell sources and biomaterials provided excellent potential for emulating *in vivo* microenvironments, producing self-organized cell structures *in vitro*[8,9]. While stem cell-derived cardiac organoid models exhibit remarkable developmental and contractile properties, they require over 10 days to mature before being suitable for drug screening. Additionally, prolonged differentiation often results in immature or heterogeneous phenotypes, which can introduce variability in drug responses[10]. Moreover, stem cell-based organoids' implementation difficulties and exorbitant expenses have restricted their further applications in high-throughput drug screening. Hence, an MF model with multi-cell types that is easily accessible is urgently needed. Growing research has inspired more and more focus on monocytes and macrophages in fibrosis development[11]. Therefore, macrophage-consisting 3D myocardial tissue possesses high levels of clinical replicability and is easy to manage for reliable screening of candidates with anti-fibrosis activity.

The resins of *T. vernicifluum*, a traditional Chinese medicine, originate from the resin stored in the phloem of lacquer trees and secreted when damaged by external stimuli due to its self-injury-repair mechanism characteristics[12]. Current studies have proved that *T. vernicifluum* has multi-pharmacological effects such as anti-inflammation, antioxidation, and promoting blood circulation[13-15], and is widely used in treating fibrotic diseases[16-18]. Therefore, compounds in *T. vernicifluum* provide a natural library of candidates for the treatment of MF.

Herein, a 3D fibrosis model of myocardial tissue was pioneered by integrating multi-cell types, *i.e.*, primary CMs, CFs, and bone-marrow-derived macrophages (BMDMs). The cell types and proportions are in precise control with good stability, high sensitivity, and a short cultivation period, which fits the drug screening. Collagen was incorporated as a supportive hydrogel to facilitate the contractile phenotype in response to activated fibroblasts, and a visualized readout for candidates screening[19,20]. After establishing the 3D fibrosis model of myocardial tissue under hypoxia, 76 compounds extracted from *T. vernicifluum* were screened for anti-cell proliferation and anti-3D myocardial tissue contraction. After evaluation using both classic 2D−TGF-β−CFs and 3D myocardial tissues, representative compounds with anti-MF capabilities were subsequently validated using mice subjected to left anterior descending coronary artery (LAD) ligation, demonstrating that the 3D myocardial tissues offer improved accuracy for phenotypic screening of anti-MF candidates (Fig. 1). Finally, a novel clinic-relevant, sensitive, quantifiable, content-defined, and visualizable 3D myocardial tissue was established. Furthermore, two bioactive compounds exhibiting potent anti-fibrotic effects were identified as promising drug candidates for MF therapy.

2. Materials and methods

2.1. Animals and ethics statement

All experiments involving animals were conducted in accordance with the ethical standards set out by the Animal Ethics Committee of Beijing University of Chinese Medicine (Approval No. BUCM-2023041103-2014) and in compliance with the "Guidelines for the Care and Use of Laboratory Animals" published by the National Institute of Health (NIH Publication No. Resolution No. 85-23, revised 1996). Sixty healthy male Institute of Cancer Research mice (28 ± 2 g, 8-week-old), 20 healthy Sprague−Dawley (SD) rats (1−3-day-old), and 20 healthy SD rats (10-day-old) of specific pathogen-free grade were obtained from Beijing Spefo Technology Co. (Beijing, China). The feeding conditions for the mice were 12 h light−dark cycle, humidity of 55 ± 5%, constant temperature of 25 °C, and adaptive feeding for 3 days before the experiments. Animals were humanely killed as needed to reduce suffering and were not fed the night before they were killed.

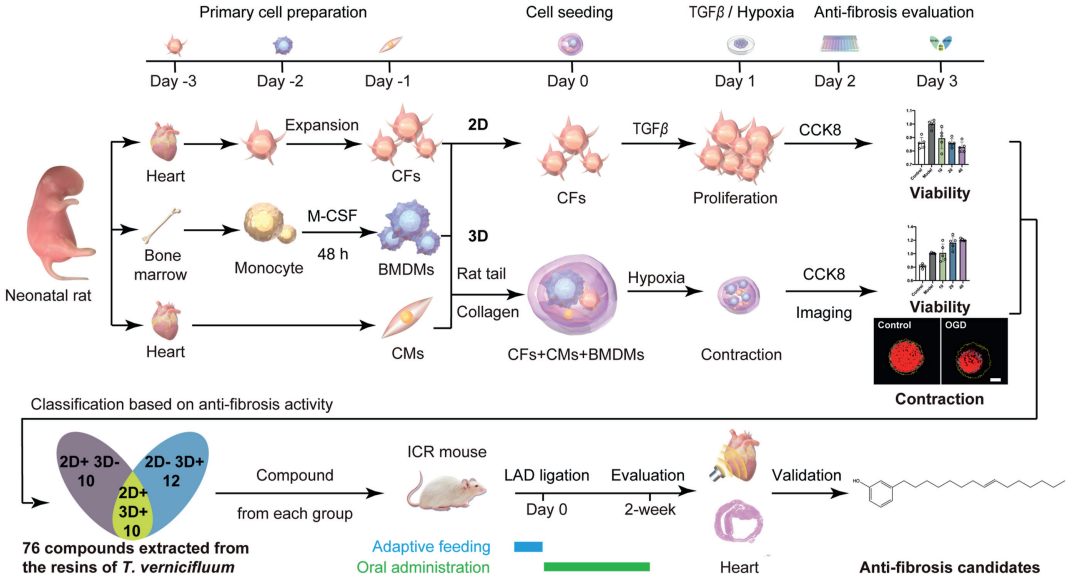

Figure 1 Experimental schematic of the construction and application of the contractile 3D myocardial tissue. Schematic of isolation of cardiac fibroblasts (CFs), bone-marrow-derived macrophages (BMDMs), and cardiomyocytes (CMs) from neonatal rats. Cocultured CFs, CMs, and BMDMs were encapsulated in collagen hydrogel and formed 3D myocardial tissue under hypoxic conditions. CFs were cultured on conventional two-dimensional (2D) plates and used as a fibrosis model upon TGF-β treatment. 3D−OGD−MF and 2D−TGF-β−CFs were used to screen 76 compounds extracted from the resins of *T. vernicifluum*. Compounds with anti-fibrotic activity based on the contraction of the 3D-oxygen-glucose deprivation (OGD)-MF and proliferation of 2D−TGF-β−CFs were classified into $3D^+$ group and $2D^+$ group, respectively. Compounds from $2D^+3D^-$, $2D^-3D^+$, and $2D^+3D^+$ groups were subjected to mice with left anterior descending coronary artery (LAD) ligation for further validation. After 2-week of administration of specific compounds, mouse hearts were analyzed for function and organization.

2.2. *Drugs*

The resins of *T. vernicifluum* were collected from Anguo City, Hebei Province, China. The sample (No. GQ201909) is stored in the specimen bank of the Center for Modern Research of Traditional Chinese Medicine, Peking University.

Extraction and separation process: a total of 50.3 kg of the resins of *T. vernicifluum* was extracted 3 times with 95% ethanol under reflux for 2 h each time. The combined filtrate was concentrated under reduced pressure to yield 2.2 kg of crude extract. This extract was suspended in water and successively partitioned 3 times with petroleum ether, ethyl acetate, *n*-butanol, and water, yielding 1123 g of petroleum ether extract, 780 g of ethyl acetate extract, 77 g of *n*-butanol extract, and 185 g of aqueous extract. Using column chromatography and spectroscopic techniques, 76 compounds were isolated and identified from the petroleum ether and ethyl acetate fractions for further bioactivity screening.

For screening, the isolated compounds were dissolved in dimethyl sulfoxide to prepare a 20 mmol/L stock solution, which was further diluted with culture medium before use. In the treatment of mice with LAD ligation, compounds were suspended in sodium carboxymethyl cellulose and administered orally at a dose of 10 mg/kg.

Fosinopril (Shi Guibao Pharmaceutical, Shanghai, China), a prescription drug used for treating heart failure and hypertension, was used as a positive drug in this animal study at a concentration of 10 mg/kg.

2.3. *Reagents*

Reagents used in this research included papain (Sigma, St. Louis, MO, USA), recombinant rat macrophage colony stimulating factor (M-CSF, Novoprotein, Suzhou, China), recominant human TGF-β (Peprotech, Cranbury, NJ, USA), SB431542 (Selleck, Houston, TX, USA), minimum essential medium (MEM, HyClone, Cleveland, OH, USA), fetal bovine serum (FBS, Corning, New York, NY, USA), phosphate buffered saline (PBS, Gibco, Carlsbad, CA, USA), penicillin/streptomycin solution (Gibco), 0.25% trypsin−EDTA (Gibco), calcein-AM (Amresco, Radnor, PA, USA), propidium iodide (PI, Biofount, Beijing, China), Hoechst 33342 staining solution for live cells (Hoechst 33342, Beyotime, Shanghai, China), bovine serum albumin (Absin, Shanghai, China), Triton X-100 (Biosharp, Tianjin, China), 1,1′-dioctadecyl-3,3,3′,3′-tetramethylindocarbocyanine perchlorate (DiI, Beyotime), radio immunoprecipitation assay (Applygen, Beijing, China), bicinchoninic acid (BCA, Applygen), TRIzol reagent (Ambion, Austin, TX, USA), diethylpyrocarbonate (DEPC) water (Invitrogen, Carlsbad, CA, USA), SYBR Green Master (Invitrogen), cell counting kit-8 (CCK-8, Dojindo, Tokyo, Japan), and paraformaldehyde (PFA, Aladdin, Shanghai, China).

2.4. *Isolation and culture of primary cells*

Primary CMs and CFs were isolated from 1−3-day-old SD rats. The shredded myocardial tissue was digested with 0.15% papain in water at 37 °C. CFs were separated from CMs by differential adhesion for 90 min. CMs and CFs were cultured in MEM supplemented with 10% FBS in a humidified incubator with 5% carbon dioxide (CO_2) at 37 °C. CFs in passages 2−5 were used for further experiments.

For the isolation of BMDMs, 10-day-old SD rats were initially sterilized in beakers containing 75% ethanol for 1 min. The tibiae and femurs of the rats were separated on ice and the bone marrow was squeezed into a solution containing 1 mL of MEM

supplemented with 10% FBS, 1% penicillin/streptomycin solution, and M-CSF at a concentration of 10 μg/mL. Subsequently, the erythrocyte lysis solution was added and the mixture was incubated at 4 °C for 10 min, before being centrifugated at 1000 rpm (1-15K, Sigma, Osterode am Harz, Germany) for 5 min. The pellet was resuspended in MEM and transferred to a T-25 culture flask. After 1 h, the supernatant was collected and transferred to another T-25 culture flask, with the medium solution in the latter renewed halfway through the incubation period.

For hypoxia culture, the cells were maintained in a tri-gas incubator with 1% oxygen, 5% CO_2 and 94% nitrogen.

2.5. Preparation of collagen hydrogels

The tails were split from SD rats and sterilized in 75% ethanol for 2 h. The silky silver tendon was dissolved in 0.1% acetic acid by stirring at 4 °C for 2 days. After centrifugation at 16,000×*g* for 90 min, collagen in the upper clear solution was reserved for further experiments.

Before cell seeding, collagen solution, 10 × PBS, distilled water, and 1 mol/L NaOH were prechilled on ice. After thoroughly mixing collagen in PBS to the desired concentration and adjusting pH to 7.0 using NaOH, the cell suspension was mixed with hydrogel quickly. Then the mixture of cells and neutralized collagen solution were placed into the 96-well plate and incubated at 37 °C for 1 h to promote gel formation before adding medium.

2.6. Staining and imaging

For live/dead staining, cells were washed twice with PBS and then incubated with the dye mixture (2 μL calcein-AM and 3 μL PI in 1 mL PBS) for 10 min at 37 °C. Subsequently, the living cells and apoptotic cells were observed and imaged using a confocal microscope (Leica, Wetzlar, Germany).

For the visualization of cocultured cells, cells and dyes, *i.e.*, CMs in Hoechst 33342 (10 μL Hoechst 33342 in 1 mL PBS), CFs in calcein-AM (2 μL calcein-AM in 1 mL PBS), and BMDMs in DiI (10 μL DiI in 1 mL PBS) were incubated respectively for 20 min at 37 °C before seeding. Then, cells were washed with PBS twice and mixed with collagen to form the 3D cardiac tissues. After 24 h, the 3D cardiac tissues were observed and imaged using a Leica confocal microscope.

For immunostaining, cells in 2D and 3D cultures were fixed with 4% PFA (pH = 7.4). After treatment with 5% bovine serum albumin and 0.3% Triton x-100, the cells were incubated overnight at 4 °C with primary antibodies and then for 1 h at 37 °C with secondary antibodies. Cells were observed under the high-content analysis system (BD Biosciences, San Jose, CA, USA). The antibodies and dyes used were as follows: anti-vimentin antibody (Origene, Rockville, MD, USA, 1:250), anti-alpha smooth muscle (α-SMA) antibody (Abcam, Cambridge, England, 1:250), DAPI (Abcam, 1:200), goat anti-rabbit IgG (Cohesion Biosciences, London, England, 1:200) and goat anti-chicken IgG (Cohesion Biosciences, 1:200).

2.7. Western blot (WB)

A total cellular protein extraction was conducted using radioimmunoprecipitation assay lysis buffer. The protein content in each extract was determined using a bicinchoninic acid assay, after which the samples underwent sodium dodecyl sulfate-polyacrylamide gel electrophoresis. The samples were boiled and loaded onto a 10% sodium dodecyl sulfate-polyacrylamide gel for electrophoresis at 120 V for 80 min. Following electrophoresis, the protein fractionated on the gel underwent transfer to the nitrocellulose membrane. This was achieved by electrorotation at 300 mA for 90 min. Following this, the membrane was incubated with primary antibodies at 4 °C for 12 h, then incubated with secondary antibodies at room temperature for 2 h, and imaged using an imager (Bio-Rad, Hercules, CA, USA) after incubation with enhanced chemiluminescence detection reagent at room temperature for 1 min. The band densities were analyzed and quantified using ImageJ software. The antibodies used for WB were as follows: anti-α-SMA antibody (Abcam, 1:1000), anti-collagen III (Col III) antibody (Abcam, 1:1000), anti-GAPDH antibody (Abcam, 1:10,000), HRP anti-rabbit IgG antibody (Abcam, 1:10,000), and rabbit anti-mouse IgG H&L (Abcam, 1:10,000).

2.8. Real-time reverse transcription-polymerase chain reaction (RT-PCR) analysis

Total RNA was extracted with TRIzol reagent. The quality and integrity of the RNA were determined using the NanoDrop 2000 (Thermo Scientific, Waltham, MA, USA). cDNA synthesis was performed using a RevertAid first-strand cDNA synthesis kit (Thermo Scientific). The mRNA level was detected using a PCR supermix kit (Vazyme, Nanjing, China). Expression of *GAPDH* was employed as an internal control. The primer sequences of the target genes *ACTA2*, *COL3A1*, matrix metalloprotein 9 (*MMP9*), and *GAPDH* are listed in Supporting Information Table S1 (Sangon Biotech, Shanghai, China). The relative expression levels of the target genes were calculated using the $2^{-\Delta\Delta Ct}$ method.

2.9. Flow cytometry detection

The cells were enzymatically digested for 40 s to form a single-cell suspension. After centrifugation, the cells were washed with PBS and incubated with antibodies on ice for 40 min. After washing twice, cells were suspended in 300 μL PBS and then detected by flow cytometry (BD Biosciences). The antibodies were as follows: anti-Siglec1/CD169 (Santa, Dallas, TX, USA, 1:50), anti-Vimentin antibody (Abways, Shanghai, China, 1:50), and anti-α-actinin (Proteintech, Rosemont, IL, USA, 0.4 μg per 10^6 cells in a 100 μL suspension).

2.10. Cell viability detection

Cell viability in 2D and 3D cultures was measured using CCK-8 according to the manufacturer's instructions. In brief, 10 μL of CCK-8 was added to the wells and incubated at 37 °C for 2 h. The optical density of the cells in each well was then measured using a microplate reader (PerkinElmer, Waltham, MA, USA) set to a wavelength of 450 nm.

2.11. Compound screening

In screening, the relative proliferation of cells in 2D or 3D culture after treatments was calculated as $A_{450\ \text{compound}}/A_{450\ \text{model}}$ using data from CCK-8 assay. A compound was designated as a candidate with anti-fibrotic activity if its relative proliferation value was less than 1.

The relative contraction of myocardial tissue in 3D culture after treatments was calculated as $Area_{model}/Area_{compound}$ using data from live/dead staining assay. A compound was designated as a candidate with anti-fibrotic activity if its relative contraction value was less than 1.

2.12. Animal model of MF

MF was induced in mice by ligature of the LAD coronary artery. Following anesthesia by intraperitoneal injection of 0.5% sodium pentobarbital (50 mg/kg), the animal ventilator was connected, and the procedure was carried out in the third/fourth rib area on the left side of the chest. The left anterior descending coronary artery was ligated 1−1.5 mm distal to the left auricle. The immediate lightning of the cardiac tissue at the ligation site was considered a sign of successful surgery. Mice that underwent open-chest surgery but did not receive LAD ligation were part of the sham group.

2.13. Echocardiographic assessment

After 14 days of drug administration, mice were anesthetized with isoflurane, and fixed in the supine position on the ultrasound bench. The long and short axes of the hearts of each group of mice were imaged using a mouse ultrasound probe at the papillary muscle adjacent to the left sternum. During the acquisition process, the heart rate of the mice was maintained between 450 and 550 beats per minute, and at least 10 cardiac cycles were recorded in the long and short axis regions at each measurement point. The thickness of the anterior and posterior wall of the left ventricle was measured during diastole and systole, respectively. The left ventricular ejection fraction and left ventricular fractional shortening values were calculated using Vevo 2100 ultrasound data analysis software.

2.14. Transcriptomic sequencing and data analysis

The mice hearts were rapidly and manually separated from each carcass, immediately flash frozen in liquid nitrogen, and stored at −80 °C until RNA extraction. RNA extraction and sequencing using Illumina Novaseq X plus series of samples were performed by Beijing Novozymes Co. (Beijing, China). Sequencing reads were mapped to reference genomes GRCm38 (mm10) using HISAT2 v2.0.5 with default parameters. Gene-level expression was estimated as fragment per kilobase of transcript per million mapped reads (FPKM). Differentially expressed genes (DEGs) were identified by Limma 3.58.1 using filtering thresholds of P value < 0.05 and absolute value ($\log_2$fold change) ≥ 1. Gene ontology (GO), kyoto encyclopedia of genes and genomes (KEGG), and gene set enrichment analysis (GSEA) enrichment of DEGs were performed using cluster Profiler 4.10.0. The plots were drawn using pheatmap 1.0.12, gggsea 0.1.0, GOplot 1.0.2 and enrichplot 1.22.0.

The RNA-seq sequencing and processed data were deposited in GEO (GSE275028).

2.15. Histological examination and analysis

After completing the abdominal aorta blood collection, the mouse heart was quickly removed from the chest cage and placed in prechilled PBS to remove blood. Then the pericardium, atria, and appendages of the heart were removed. The heart tissue above the ligation line is fixed in a 4% PFA solution for further staining and imaging. The part below the ligation line was divided into 2 parts with the same volume and kept at −80 °C for subsequent experiments.

For tissue organization analysis, cardiac tissue was embedded in kerosene, sectioned at a thickness of 3−5 μm, and stained in accordance with the established hematoxylin-eosin staining protocol[21]. The evaluation of histomorphology and collagen deposition of all heart sections was performed in a double-blind manner by a pathologist who was unaware of the experimental setup.

In an analysis of collagen deposition, heart slices were stained using Sirius-red and imaged under polarizing microscopy. Owing to differential birefringence, Col I, and Col III were observed in bright shades such as orange and green.

2.16. Enzyme-linked immunosorbent assay

Blood samples from mice were collected from the abdominal aorta with a sterile 1 mL disposable syringe and allowed to coagulate at room temperature for 2 h. The samples were centrifugated at 855×g for 10 min at 4 °C. After centrifugation, the supernatant was collected for enzyme-linked immunosorbent assays of procollagen III C-terminal propeptide (PIIICP, Keborui, Shanghai, China) and Galectin-3 (Cohesion Biosciences) levels.

2.17. Molecular docking

The crystal structures of the proteins used for docking were obtained from the RCSB PDB database[22]. Energy minimization of 2 molecules was carried out under the MMFF94 force field.

Molecular docking was carried out using AutoDock Vina 1.2.3 software according to instructions[23]. Briefly, the receptor proteins were processed using PyMol 2.5.52 to remove the water molecules, salt ions, and small molecules. Then the docking box was set up so that it wrapped around the entire protein structure. Molecules and proteins were converted to the PDBQT format using ADFRsuite 1.03. The exhaustiveness of the global search was set to 32 and the rest of the parameters remained at their default settings. The output with the highest scores was considered to be the binding conformation. The docking results were also visualized using PyMol 2.5.52.

2.18. Statistical analysis

Quantitative data were analyzed using Graph Pad Prism 9 and shown with the mean ± standard deviation (SD). One-way ANOVA was used to calculate differences between groups. Differences between groups were considered statistically significant if $P < 0.05$.

3. Results

3.1. Primary CMs, CFs, and BMDMs formed 3D myocardial tissue in collagen hydrogel

To achieve a rapid and sensitive phenotypic screening of anti-fibrotic compounds, we extracted CMs, CFs and BMDMs from neonatal rats to improve contractile responses. Primary CMs and CFs were isolated from the heart of 1−3-day-old rats by differential velocity adhesion[24,25]. BMDMs were obtained after 48 h of activation by M-CSF of monocytes, which were extracted from the bone marrow of 10-day-old rats[26]. Applying a well-established protocol for primary cell isolation, around 99.8% of primary CMs

expressed α-actinin[27], 99.9% of primary CFs expressed vimentin and 98.2% of primary BMDMs expressed CD169 in the isolated populations as identified using flow cytometry[28,29] (Fig. 2A−C, Supporting Information Fig. S1). We then utilized primary CMs, CFs, and BMDMs with high purity to construct 3D myocardial tissue.

In 3D myocardial tissue, collagen was used as an extracellular matrix to support and stabilize the formation of spheres. To determine the optimal collagen concentration for 3 kinds of cells in coculture, collagen hydrogels with a gradient of 1−3 mg/mL were tested for the viability of each cell. For CMs and CFs, cell viability was kept as high as ∼99% in all the collagen hydrogel groups. For BMDMs, however, cell viability decreased significantly along with growing collagen concentrations (Fig. 2D−F). Therefore, collagen with 1 mg/mL was applied for multicellular 3D myocardial tissue formation.

Primary CMs, CFs, and BMDMs were mixed using a 1:1:1 ratio and kept in collagen hydrogel (1 mg/mL) for as long as 7 days according to the previous studies[30,31]. The good cell viability and multilayered structure of 3D myocardial tissue in long-term culture was visualized using fluorescence imaging on Day 5 (Fig. 2G). Using the live cell staining method, we can observe a mixture of 3 kinds of cells and their interactions in 3D myocardial tissue, which would facilitate cross-talks in response to the hypoxia microenvironment (Fig. 2H).

3.2. Oxygen-glucose deprivation (OGD) induced a fibrotic phenotype of 3D myocardial tissue

To better replicate the fibrotic progression *in vivo*, we utilized TGF-β and OGD treatments, which are established methods for *in vitro* MF models. TGF-β and OGD treatments were applied to CFs and myocardial tissue (cocultured CFs, CMs and BMDMs) in 2D and 3D culture respectively, resulting 5 groups named 2D−TGF-β−CFs, 2D−TGF-β−MF, 2D−OGD−CFs, 2D−OGD−MF and 3D−OGD−MF (Fig. 3A). After 24 h of TGF-β treatment, the cell viability of individual CFs in 2D culture was significantly higher when compared to the control group. However, in the 2D−TGF-β−MF system, cell viability showed no increase compared to the control group after 24 h of treatment due to the contrasting responses of CFs and macrophages to TGF-β[32]. Following an 8-h OGD treatment, 2D−OGD−MF and 3D−OGD−MF displayed a significant increase in cell viability, whereas 2D−OGD−CFs viability remained unvaried compared to the control. This illustrates the vital need for crosstalk between CFs and BMDMs in hypoxia-induced fibrosis. Furthermore, immunofluorescence staining of α-SMA$^+$ cells revealed a greater concentration in the 2D−TGF-β−CFs, 2D−OGD−MF, and 3D−OGD−MF groups than in the other groups (Fig. 3B). 3D−OGD−MF showed an advantage over 2D−OGD−MF, because the contraction of hydrogel in 3D−OGD−MF was easily observed and quantified along with fibrosis progression using fluorescence imaging (Fig. 3C), proposing a rapid and low-cost strategy for high-throughput screening of anti-fibrotic candidates.

To further verify the cell fibrosis in 3D−OGD−MF, we assessed the levels of fibrotic markers in total cells in 3D myocardial tissue using RT-PCR, WB, and immunofluorescence. The upregulated mRNA expression of *ACTA2*, *COL3A1*, and *MMP9*, coupled with increased protein expression of α-SMA and Col III indicated that OGD-activated fibrosis in 3D myocardial tissue (Fig. 3D−F). In the 3D−OGD−MF model, the staining of α-SMA and Vimentin showed a greater number of fluorescence signals and higher co-localization ratios, suggesting enhanced fibrotic activation of CFs in 3D−OGD−MF compared to the control (Fig. 3G).

To investigate the interactions among the 3 cell types, 3D−OGD−MF and 3 types of 2D-cultured cells at a ratio of 1:1:1 were subjected to RNA-seq. There were 462 differentially expressed mRNAs between 3D myocardial tissues and 2D cells, of which 363 were upregulated and 99 were downregulated (Supporting Information Fig. S2A). GO analyses showed that DEGs were enriched in innate immune response, inflammatory response, and immune effector process (Fig. S2B). The enriched KEGG pathways mainly included the JAK−STAT signaling pathway, NF-κB signaling pathway, IL-17 signaling pathway, and TNF signaling pathway (Fig. S2C). Expression of genes related to cell death, for example, *NLRP3*, genes related to immune response, such as *NFKB1*, *NFKB2*, *IL1A*, *IL1B*, *IL6*, and genes related to fibrosis, such as *MMP3*, *MMP9*, *MMP12*, and *COL6A6* were significantly up-regulated (Fig. S2D). The RNA-seq results indicate that intercellular interactions in 3D myocardial tissue permeate the inflammatory response and fibrotic process under OGD.

3.3. Phenotypic screening of compounds extracted from T. vernicifluum revealed anti-fibrotic candidates

The resins of *T. vernicifluum*, a processed dry product of the resins of the anacardiaceae plant, showed a high molecular complexity as shown in the fingerprint of petroleum ether extract (Fig. 4A and B, Supporting Information Fig. S3). 76 compounds obtained from ethyl acetate extract and petroleum ether extract from *T. vernicifluum* resins, were screened for anti-fibrotic potential using 3D myocardial tissue and 2D−TGF-β−CFs. 3D myocardial tissues were seeded into 96-well plates at 20 μL per well and stimulated with OGD to induce a fibrotic effect for 8 h. Similarly, 2D CFs were seeded into 96-well plates and induced with TGF-β at 20 μmol/L. The 2D−TGF-β−CFs model was included in the following screening assays as a control model of fibrosis. Both 2D and 3D cultured cells were treated with compounds extracted from *T. vernicifluum*, as well as SB431542, a well-established TGF-β inhibitor with demonstrated anti-fibrotic effects, serving as a positive control.

For 3D myocardial tissue, the morphology of each tissue before and after treatments was stained and analyzed using ImageJ. Following OGD treatment, the 3D myocardial tissue in the model group without additional compounds experienced a contraction resulting in a reduction of their diameter by half. Meanwhile, the 3D myocardial tissue of the positive control group with SB431542 remained the same. Among 76 screened compounds, 26 demonstrated inhibitory effects on tissue contraction (Fig. 4C and D). The proliferation of 3D−OGD−MF with compound treatment was assessed using CCK-8 to confirm their anti-fibrotic effects (Fig. 4E). 26 compounds, which showed anti-fibrotic activity following the observation based on contraction assays, also exhibited the ability to decrease proliferation (Fig. 4F). These 26 compounds fell into the categories of urushiols and flavonoids, and were labeled as 3D$^+$ compounds (Fig. 4G, Supporting Information Table S2). To rule out the possibility that drug toxicity was the cause of the decrease in cell survival rate, cytotoxicity tests were conducted on 76 compounds from *T. vernicifluum*. Among 76 compounds, only 4 compounds showed significant cellular toxicity at 20 μg/μL (Fig. 4H, Supporting Information Fig. S4).

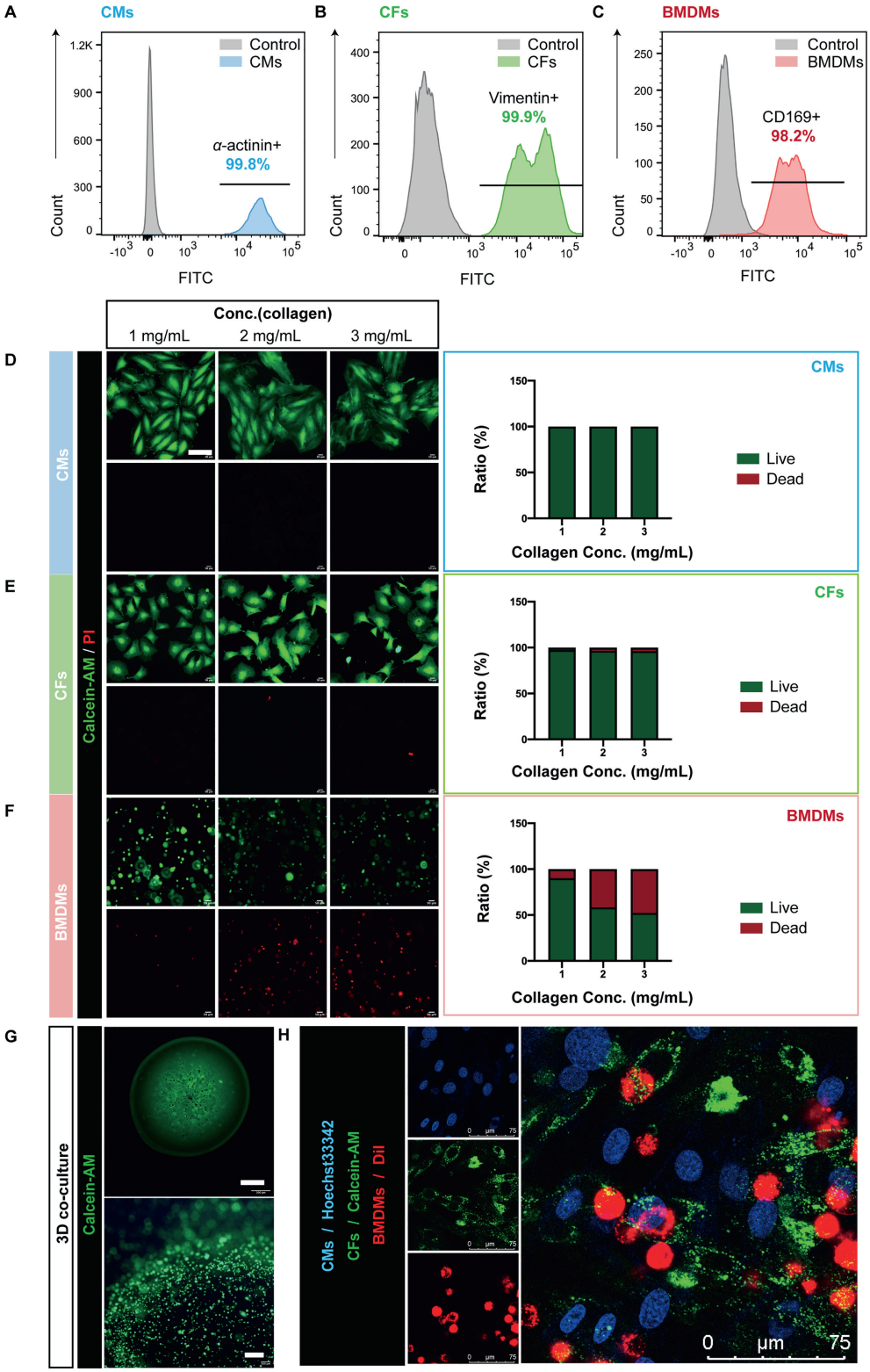

Figure 2 Construction of multicellular 3D myocardial tissue. Flow cytometric analysis of isolated (A) primary CMs using α-actinin, (B) CFs using vimentin, and (C) BMDMs using CD169. Calcein-AM and PI staining of live and dead cells of (D) CMs, (E) CFs, and (F) BMDMs in collagen hydrogel at 1, 2, and 3 mg/mL, respectively. Scale bar = 50 μm. Cell viability statistics are shown in the right lane of each figure. (G) Calcein-AM staining of living cells in 3D myocardial tissue in collagen hydrogel. Scale bar (up) = 200 μm, Scale bar (down) = 100 μm. (H) Confocal image of CMs nucleus using Hoechst 33342 live staining (blue), CFs cytoplasm using calcein-AM live staining (green) and BMDMs membrane using DiI live staining (red). Scale bar = 75 μm.

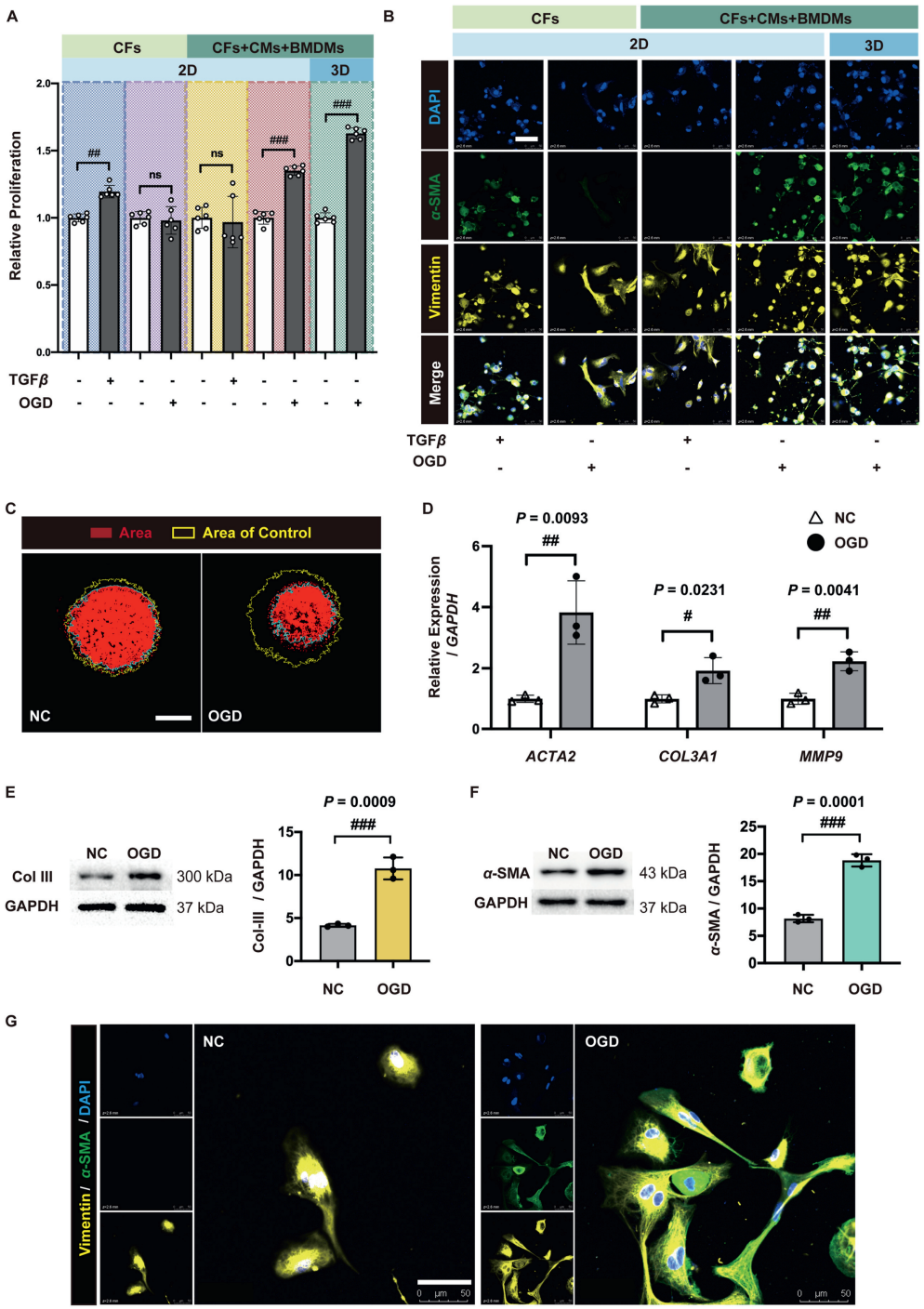

Figure 3 Hypoxia-induced fibrosis in 3D myocardial tissue models. (A) Relative cell proliferation and (B) α-SMA staining of CFs and cocultured CFs, CMs, and BMDMs in 2D and 3D culture after TGF-β or OGD treatment. Data are presented as mean ± SD, $n = 6$, $^{\#\#}P < 0.01$, $^{\#\#\#}P < 0.001$ *vs*. Control. ns, no significance. Scale bar = 50 μm. (C) The contractile phenotype of OGD-induced fibrosis in 3D myocardial tissue models. The area of calcein-AM stained 3D myocardial tissue was detected using ImageJ and labeled red for area analysis. The outer border of the 3D myocardial tissue in the control group was highlighted in yellow to visualize contractility after OGD treatment. Scale bar = 200 μm. (D) The mRNA expression level of *ACTA2*, *COL3A1*, and *MMP9* in 3D myocardial tissue models after OGD treatment. Data are presented as mean ± SD, $n = 3$, $^{\#}P < 0.05$, $^{\#\#}P < 0.01$ *vs*. Control. The protein expression level of (E) Col III and (F) α-SMA in 3D myocardial tissue models after OGD treatment. Data are presented as mean ± SD, $n = 3$, $^{\#}P < 0.05$, $^{\#\#}P < 0.01$ and $^{\#\#\#}P < 0.001$ *vs*. Control. (G) Immunofluorescence staining of α-SMA and vimentin in 3D myocardial tissue models after OGD treatment. Scale bar = 50 μm.

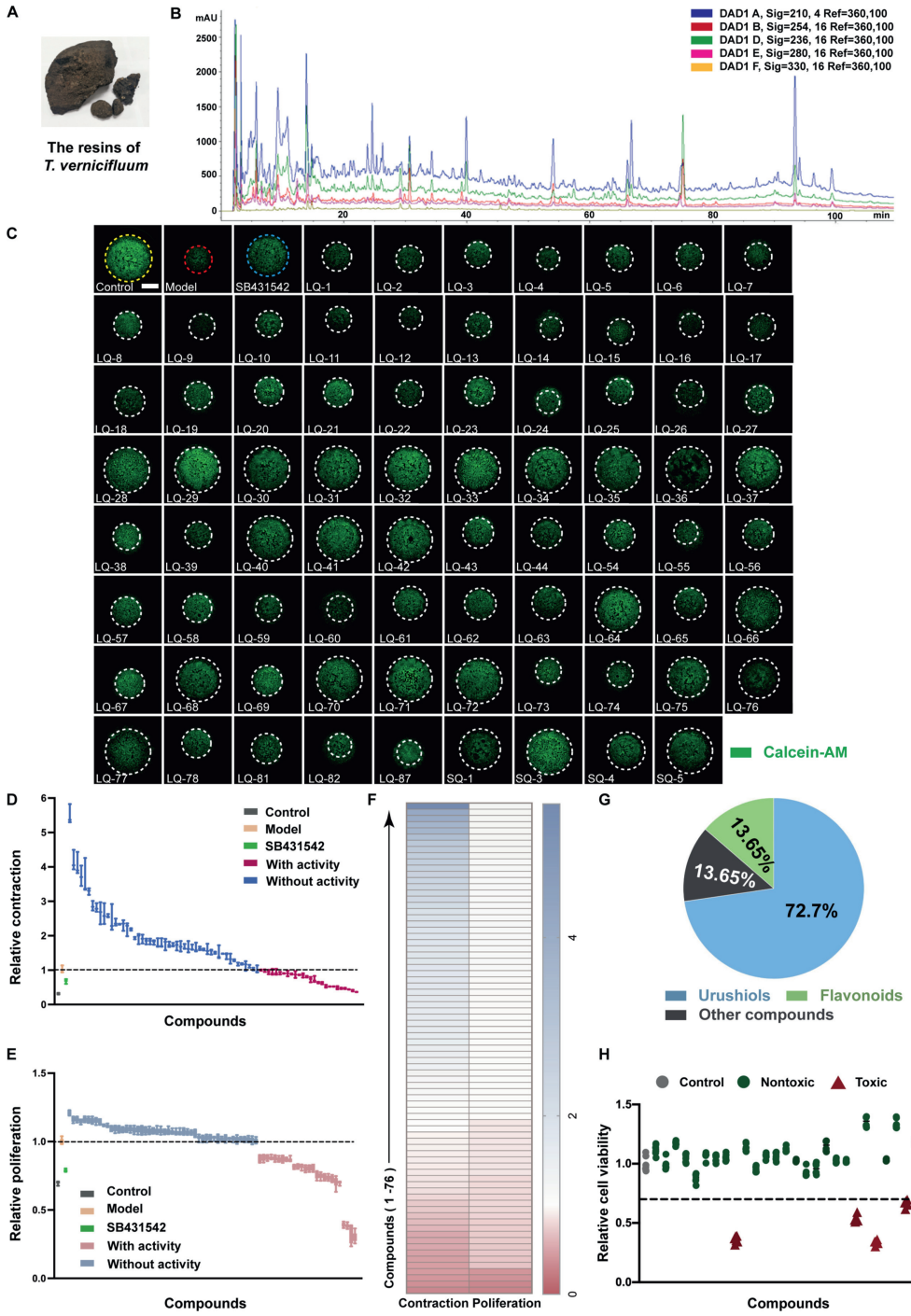

Figure 4 Phenotypic screening of anti-MF candidates using 3D myocardial tissue models. (A) Photograph of *T. vernicifluum*. (B) Multi-wavelength HPLC fingerprint of the extract of *T. vernicifluum*. (C) Representative images of calcein-AM labeled 3D myocardial tissue models after OGD and compound treatment. Scale bar = 200 μm. (D) Statistics of contraction-based $3D^+$ compounds with anti-MF activity. (E) Statistics of proliferation-based $3D^+$ compounds with anti-MF activity ($n = 6$). (F) Heatmap of cell proliferation and contraction inhibition of 76 compounds. (G) Pie chart of 26 $3D^+$ compounds classifications. (H) Toxicity statistics of 26 $3D^+$ compounds. Compounds were classified as toxic when cell viability was less than 70% after 24 h treatment ($n = 5$).

Screening using 2D−TGF-β−CFs revealed 24 anti-fibrotic compounds that inhibited cell proliferation (Fig. 5A). These compounds were categorized as urushiols, terpenoids, benzofurans, astragalus mongholicus, flavonoids, and other substances, and were designated as $2D^+$ compounds (Fig. 5B, Table S2). The disparate colors of the columns on the heatmap indicated the discrepancies in anti-fibrotic activity observed between the 2D−TGF-β−CFs and 3D−OGD−MF (Fig. 5C). To our knowledge, all $2D^+$ and $3D^+$ compounds were identified with anti-fibrotic activity for the first time. Among them, 10 compounds

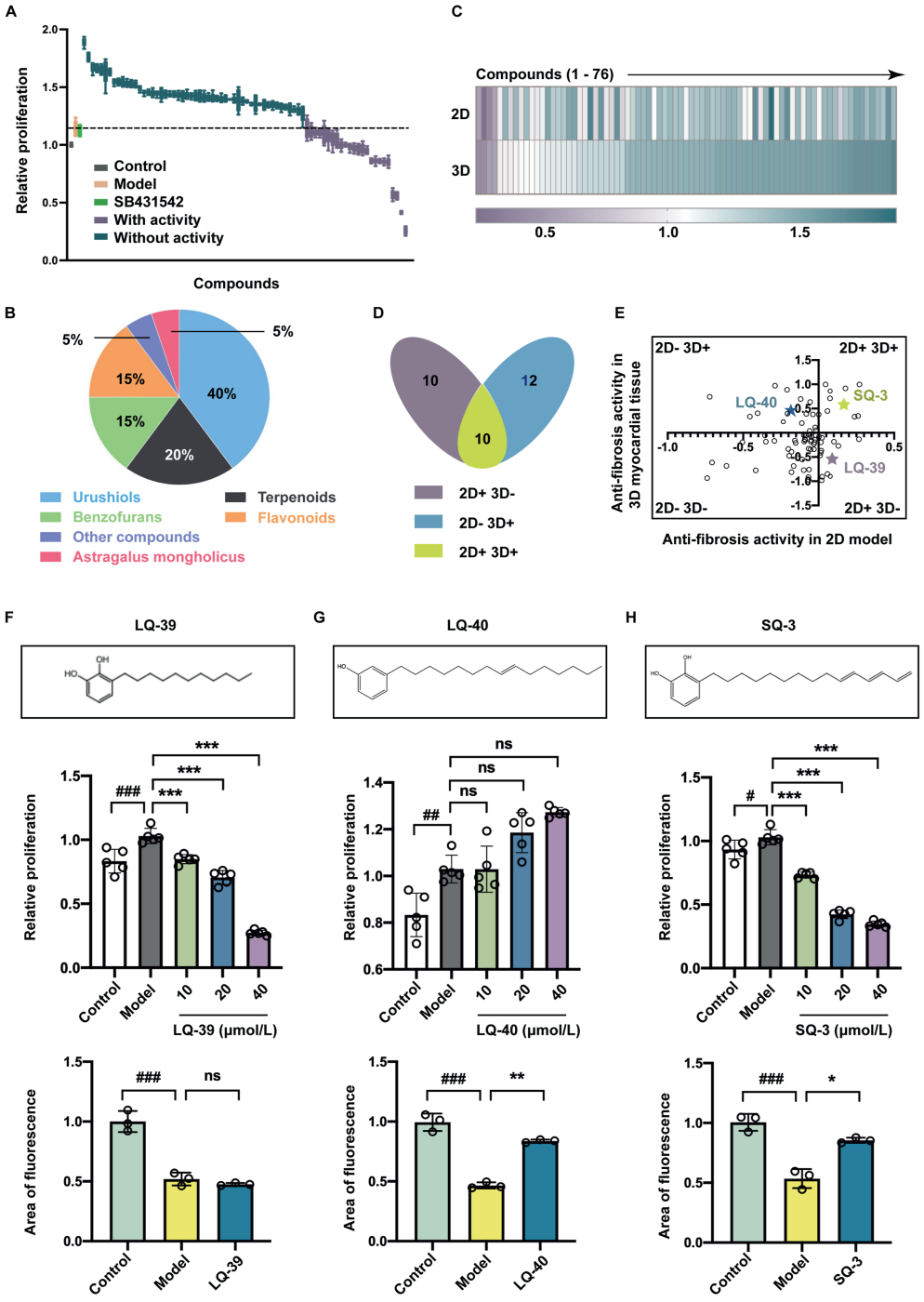

Figure 5 Different anti-MF activity uncovered using 2D and 3D models. (A) Statistics of proliferation-based $2D^+$ compounds with anti-MF compounds using 2D−TGF-β−CFs ($n = 5$). (B) Pie chart of 24 $2D^+$ compounds classifications. (C) Heatmap of cell proliferation inhibition of 76 compounds using 2D and 3D models. (D) Venn diagram of $2D^+$ and $3D^+$ compounds. (E) Inhibition distribution of $2D^+$ and $3D^+$ compounds. The structure (top), relative proliferation (medium), and area of fluorescence (bottom) of cells and tissues under (F) $2D^+3D^-$ compound LQ-39, (G) $2D^-3D^+$ compound LQ-40 and (H) $2D^+3D^+$ compound SQ-3 at gradient concentrations. Data are presented as mean ± SD, $n = 6$; $^{\#}P < 0.05$, $^{\#\#}P < 0.01$, $^{\#\#\#}P < 0.001$ *vs.* Control; $^{***}P < 0.001$ *vs.* Model. ns, no significance. In analysis of the area of fluorescence, Data are presented as mean ± SD, $n = 3$; $^{\#\#\#}P < 0.001$ *vs.* Control; $^{*}P < 0.05$, $^{**}P < 0.01$ *vs.* Model. ns, no significance.

showed activity in both the $3D^+$ and $2D^+$ groups, whereas 10 were exclusively active in the $2D^+$ group, and the remaining 12 were only found active in the $3D^+$ group (Fig. 5D). This consequently led to the classification of anti-fibrotic compounds into 3 groups: $2D^+3D^-$, 2D-$3D^+$, and $2D^+3D^+$. While considering the anti-fibrotic activities, volume availability, and toxicity for mouse-based validations, LQ-39 (3-undecylbenzene-1,2-diol), LQ-40 [(*E*)-3-(pentadec-8-enyl) phenol], and SQ-3 [3-((10*E*,12*E*)-pentadeca-10,12,14-trien-1-yl) benzene-1,2-diol] were chosen from each respective group (Fig. 5E). These 3 candidates are of high

content in *T. vernicifluum* and exhibit structural similarity. A multi-dose experiment was carried out with a range of 10−40 μmol/L to further validate the anti-fibrotic activity of SQ-3 and LQ-40, the $3D^+$ compound, utilizing 2D−TGF-β−CF models (Fig. 5F−H, Supporting Information Fig. S5). The results demonstrated that SQ-3 exhibits a substantial, dose-dependent inhibition effect on fibroblast proliferation in the 2D model, whereas LQ-40 showed no activity in the 2D model. The disputed outcome of LQ-39 and LQ-40 in 2D and 3D myocardial models necessitates additional confirmation *via in vivo* experiments.

3.4. LAD mouse model validated the anti-fibrotic activity of $3D^+$ compounds

Compounds LQ-39, LQ-40, and SQ-3, belonging to the $2D^+3D^-$, $2D^-3D^+$, and $2D^+3D^+$ groups, respectively, were assessed as potential therapeutics for cardiac fibrosis in 8-week-old mice with LAD ligation. The experiment involved a 14-day treatment period, followed by a comparison of heart functions and organization among the sham, model, LQ-39, LQ-40, SQ-3, and fosinopril groups (Fig. 6A). Fosinopril was used as a positive control treatment for hypoxia-ischemic myocardial injury after LAD ligation[33]. Two days after LAD, the weight of the sham group gradually increased, while the weight of the model group slowed down. After the LQ-40 or SQ-3 treatment, the weight gradually increased (Fig. 6B). The ultrasound results of the mouse heart are shown in Fig. 6C. Notably, the left ventricular ejection fraction and left ventricular fractional shortening values increased significantly in the LQ-40 and SQ-3 treated groups compared to the model group after 14 days of treatment (Fig. 6D). Furthermore, the left ventricular posterior wall and internal dimension increased following injury treatment with LQ-40 or SQ-3, while there was no significant change in the LQ-39 treated group. 2,3,5-Triphenyltetrazolium chloride staining demonstrated that the area of cardiac infarction (white) was significantly larger in the ligated left ventricle than in the sham group of mice. This area was attenuated in the LQ-40, SQ-3, and fosinopril groups, but not in the LQ-39 group (Supporting Information Fig. S6). The reduced plasma levels of PIIICP and Galectin-3 confirmed that myocardial injury could be repaired[34,35], and cardiac function recovered after treatment with LQ-40 and SQ-3 (Fig. 6E and F). Therefore, the administration of LQ-40 and SQ-3 would enhance cardiac function post-injury, whereas LQ-39 did not show any significant efficacy in treatment.

Furthermore, tissue structures of LQ-40 and SQ-3 treated hearts were improved with the ambiguous structure of central myocytes and myocardial fiber arrangement (Fig. 7A). However, the LQ-39 treated group failed to repair myocardial cell arrangement disorders or nucleus contractions. Furthermore, the count of nuclei decreased only in LQ-40 and SQ-3 treated group, indicating a decrease in inflammation (Fig. 7B). The results of Picrosirius-red staining showed that LQ-40 and SQ-3 could reduce the over-expansion of Col I fibers in mouse myocardial tissue after MF (Fig. 7C). However, LQ-39 improved Col I deposition, similar to that in model group (Fig. 7D). Immunostaining of α-actinin (a marker of CM), α-SMA (a marker of MF), and CD86 (a marker of pro-inflammatory macrophage) revealed decreased inflammation level of LQ-40 and SQ-3 treated hearts in comparison with model and LQ-39 treated group (Fig. 7E and F). Herein, the increased CMs and decreased MF staining in LQ-40 and SQ-3 treated hearts were also observed as altered cellular organizations, suggesting the promotion of cardiac regeneration.

To accurately assess the effects of LQ-40 and SQ3 on MF, and investigate the potential anti-fibrotic mechanism behind structural similarity, we performed mRNA-Seq analysis on mouse myocardial tissue in sham, model, LQ-40 and SQ-3 groups in triplicate (Fig. 8A, Supporting Information Fig. S7A−S7D). The heatmap of DEGs suggested a reversal at the transcriptional level after LQ-40 or SQ-3 treatment in comparison with the model group (Fig. 8B). A total of 30 identical genes were both up- or down-regulated after LQ-40 and SQ-3 treatment (Fig. 8C). KEGG enrichment of DEGs between LQ-40 and model, and DEGs between SQ-3 and model revealed the PI3K−Akt signaling pathway (Fig. 8D and E). Significant downregulation of representative genes in PI3K−Akt signaling pathway was observed in GSEA enrichment and the FPKM-based heatmap (Fig. 8F and G, Fig. S7E). Genes related to cell death, for example, *NLRP3*, genes related to immune response, such as *NFKB1*, *NFKB2*, *IL1A*, *IL1B*, *IL6*, and genes related to fibrosis, such as *MMP3*, *MMP9*, *MMP12*, and *COL6A6* were significantly down-regulated after LQ-40 and SQ-3 treatment (Fig. S7F and S7G). Molecular docking of LQ-40 and SQ-3 with the proteins corresponding to the genes listed in Fig. 8G revealed that both monomers might have high binding affinity to thrombospondin-1 (THBS-1/TSP-1), an adhesive glycoprotein on membrane and cytosol that is involved in the regulation of inflammation homeostasis and PI3K−Akt pathway (Fig. 8H)[36]. The docking score of LQ-40 and AQ-3 with TSP-1 was −7.327 and −5.731, respectively. The calculated binding affinity of LQ39 and TSP-1 was low (docking score = 6.029), suggesting that the number of double bonds may affect their flexibility.

LQ-40 was applied to 3D cultured cells with varying compositions to clarify the anti-inflammatory effect further. There was no significant contraction observed in the tissue of pure CMs, CFs, or BMDMs in 3D culture under hypoxia, which is consistent with the low immune and fibrotic responses shown in Fig. S2. In addition, LQ-40 demonstrated little efficacy in mitigating OGD-induced damage to CMs, indicating that LQ-40 exerts a limited regulatory influence on CMs. In contrast, impaired OGD-induced injury was observed in BMDMs after LQ-40 treatment. All multicellular 3D cultures composed of BMDMs demonstrated significant reparative effects of LQ-40 in both the contractile and proliferative dimensions, suggesting the possibility that LQ-40 inhibits cardiac fibrosis by modulating macrophages (Supporting Information Fig. S8A−S8C). In conclusion, LQ40 has the potential to bind to TSP-1, thereby reducing the immune response of macrophages triggered by the death of cardiomyocytes under hypoxic conditions. This may lead to a reduction in the proliferation and activation of myofibroblasts, and ultimately, the inhibition of fibrosis expansion, emphasizing the necessity of utilizing 3D myocardial tissue with multiple cell types in anti-fibrotic drug screening (Fig. 8I).

4. Discussion

Myocardial fibrosis, a common complication of cardiovascular diseases, is characterized by excessive collagen deposition and inflammatory infiltration that severely impairs cardiac function. The lack of reliable drug screening models limits the development of therapeutic strategies. Our study has developed a 3D myocardial tissue with mature cellular functions and defined ratios to facilitate a sensitive, fast, and visualizable screening of anti-fibrotic candidates. The novel 3D MF model integrated primary CMs, CFs, and BMDMs with collagen hydrogel to mimic *in vivo*

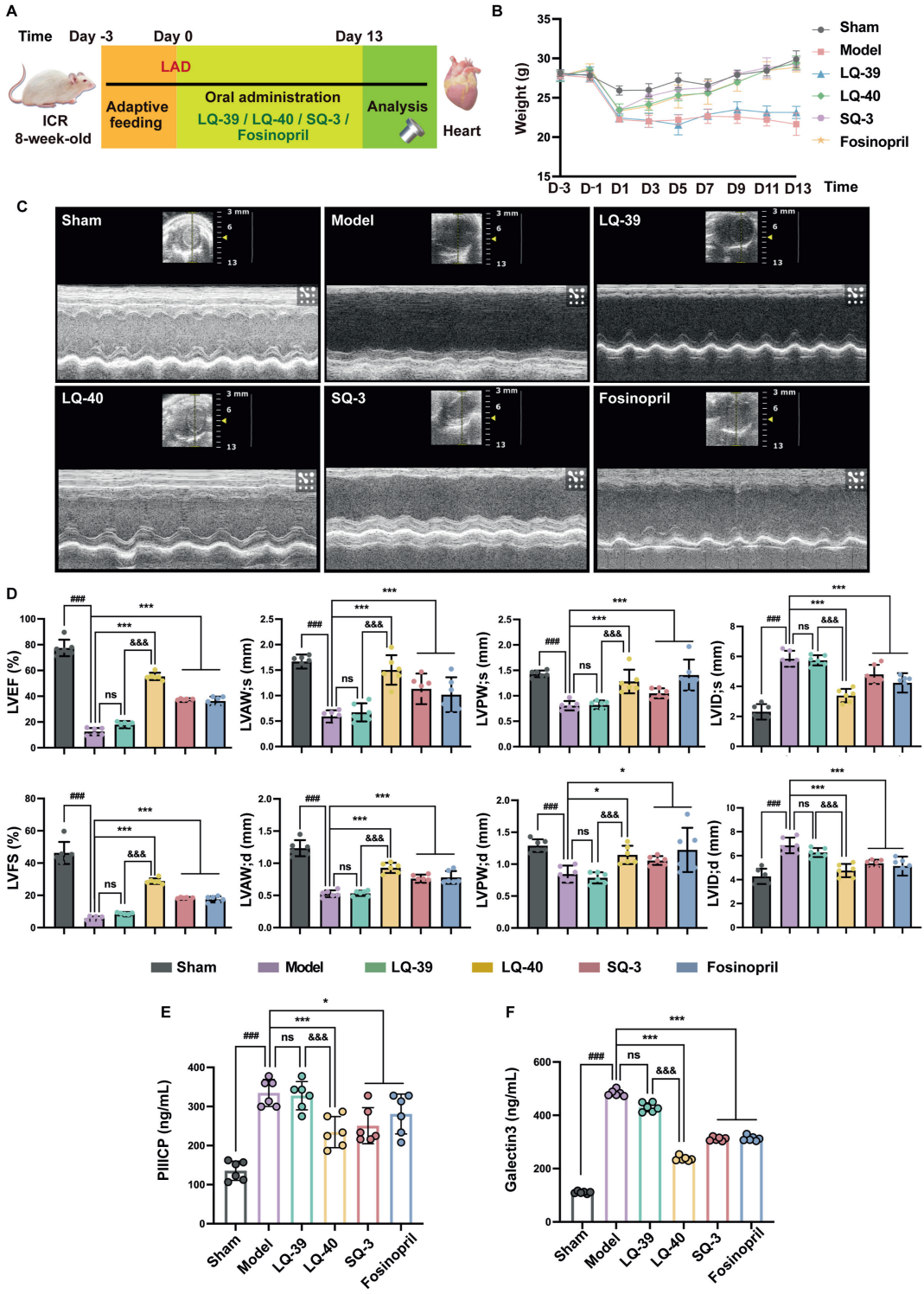

Figure 6 Validation of anti-MF activity of compounds using the mouse model with LAD ligation. (A) Schematic diagram of the experimental procedure of the study *in vivo*. (B) Weight curve of mice after LAD surgery ($n = 6$). (C) Echocardiogram. (D) Left ventricular ejection fraction, left ventricular fractional shortening, left ventricular anterior wall; systole, left ventricular anterior wall; diastole, left ventricular posterior wall; systole, left ventricular posterior wall; diastole, left ventricular internal dimension; systole, and left ventricular internal dimension; diastole analysis of mice in sham, model, LQ-39, LQ-40, SQ-3 and fosinopril group. Data are presented as mean ± SD, $n = 6$; $^{###}P < 0.001$ *vs*. Control; $^{*}P < 0.05$, $^{***}P < 0.001$ *vs*. Model; $^{\&\&\&}P < 0.001$ *vs*. LQ-39; ns, no significance. Evaluation of (E) PIIICP and (F) Galectin3 in the blood of mice from each group. Data are presented as mean ± SD, $n = 6$; $^{###}P < 0.001$ *vs*. Control; $^{*}P < 0.05$, $^{***}P < 0.001$ *vs*. Model; $^{\&\&\&}P < 0.001$ *vs*. LQ-39; ns, no significance.

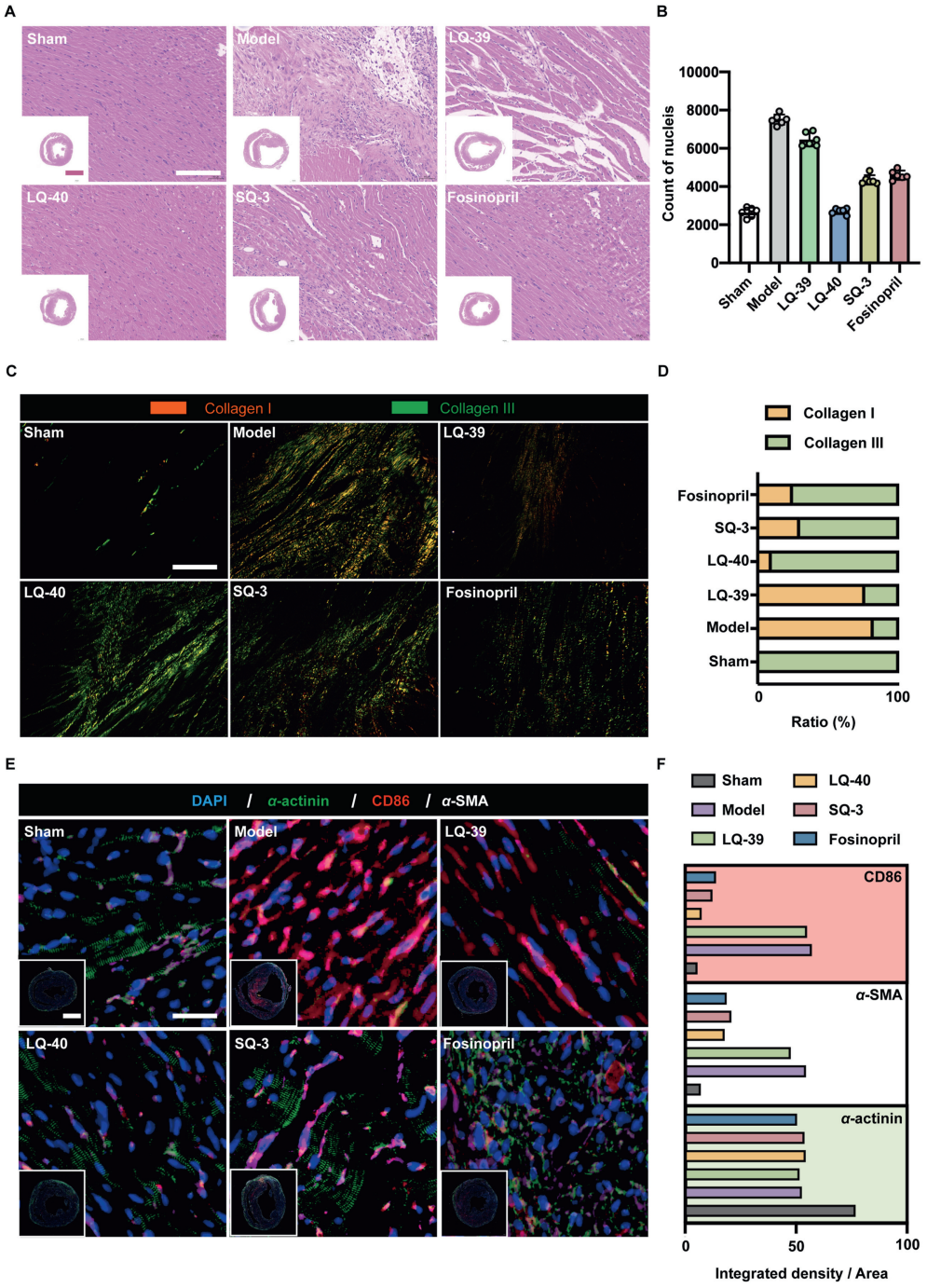

Figure 7 Tissue organization of the LAD ligation mouse model after compound treatment. (A) Hematoxylin−eosin staining of cross-sectional slices and (B) statistics of nucleus derived from the hearts of mice in each group ($n = 6$). Scale bar: 50 μm (20 × magnified region), 1 mm (original scale in lower left inset). (C) Picrosirius-red staining under polarization microscopy and (D) statistics of Collagen I (orange) and Collagen III (green) of hearts from mice in each group ($n = 3$). Scale bar = 50 μm. (E) Representative zone of immunofluorescence, and (F) statistics of α-actinin (green), CD86 (red) and α-SMA (white) of cross sections of the heart from each group. Scale bar: 50 μm (20 × magnified region), 1 mm (original scale in lower left inset).

cellular interactions between multiple cell types under hypoxia, which reduced the possibility of false-positive or false-negative screening compared to the traditional 2D−TGF-β−CF model. Using the 3D myocardial tissue model, two *T. vernicifluum* compounds, LQ-40 and SQ-3, were uncovered to have anti-fibrotic activity and then were validated using the LAD mouse model as promising candidates for MF treatment.

The 2D−TGF-β−CFs model is widely used in drug screening. Still, it has limitations as it only considers one cell type and one cytokine, neglecting the complex cellular communications contributing to pathological development. To overcome this challenge, 3D organoids have been developed with stem cell-derived multiple cell types through sequential cytokine-induced differentiation[37]. A growing number of protocols were established for stem

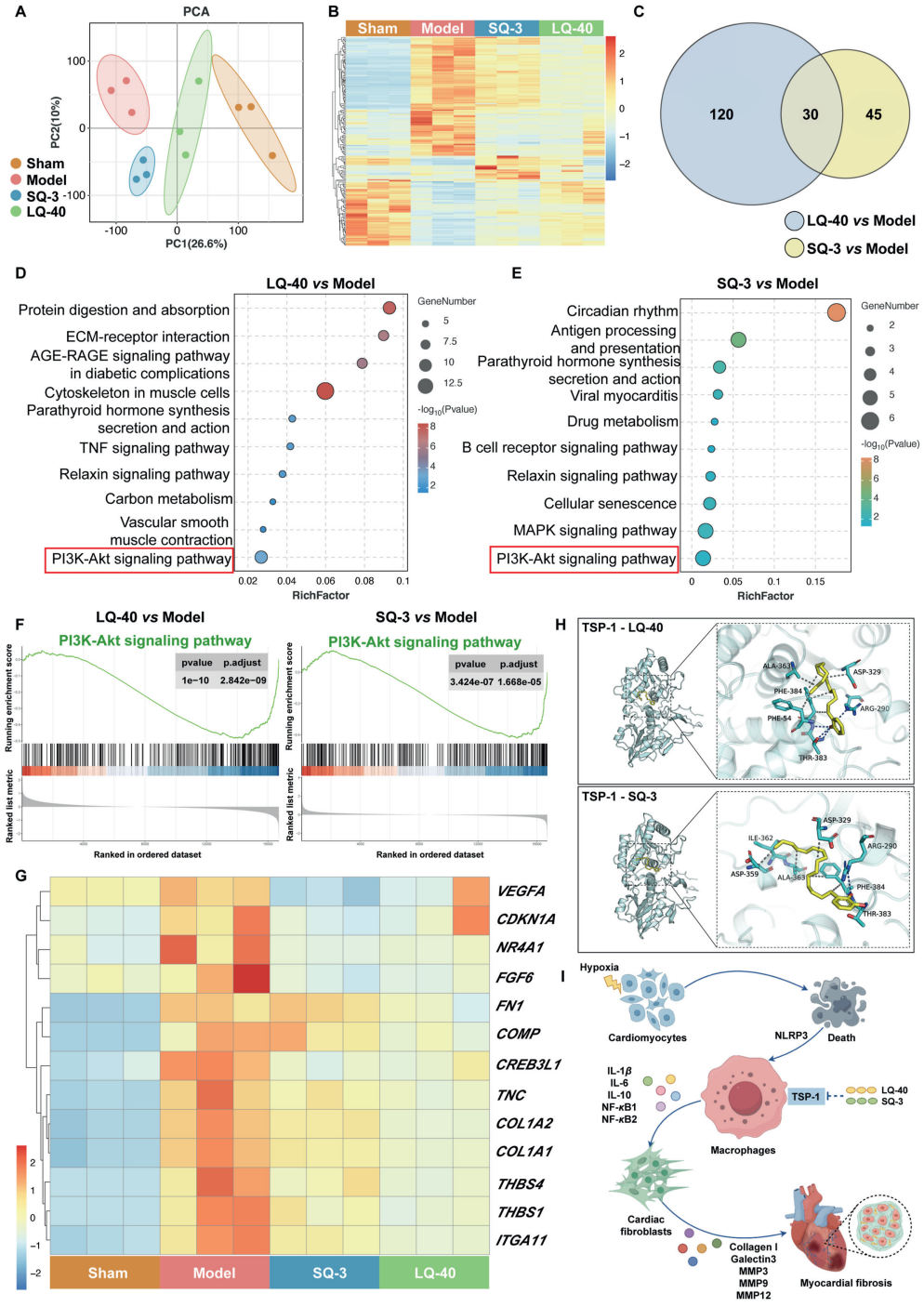

Figure 8 RNA-Seq analysis on mouse myocardial tissue in sham, model, LQ-40, and SQ-3 groups ($n = 3$). PCA plot (A) and expression heatmap (B) of RNA-Seq analysis of mouse myocardial tissue in sham, model, LQ-40, and SQ-3 groups in triplicate. (C) Venn diagrams illustrated the number of overlapping differentially expressed genes (DEGs) in LQ40 and SQ3 groups. KEGG enrichment of DEGs of LQ-40 *vs*. Model (D) and SQ-3 *vs*. Model (E) revealed the PI3K−Akt signaling pathway. (F) GSEA enrichment plot showed that gene expressions in the PI3K−Akt signaling pathway were repressed after LQ-40 (left) and SQ-3 (right) treatment. (G) Heatmap of representative DEGs enriched in PI3K−Akt signaling pathway. (H) Representative structure of the resulting TSP-1−LQ-40 and TSP-1−SQ-3 complex after computational protein-ligand docking. (I) Illustration of potential mechanisms by which LQ-40 and SQ-3 attenuate myocardial fibrosis through binding to TSP-1 and mediating intercellular crosstalk under hypoxia, highlighting the priority of upgrading to the novel 3D myocardial tissues in screening anti-fibrosis candidates.

cell-derived organoids with chambers and beating functions mimicking hearts in exploring the early development and maturation of the hearts[38]. 3D organoids are also valuable for a wide range of applications in the modeling of cardiovascular disease, as exemplified by the work of human myocardial infarction organoids and human blood vessel organoids[39-41]. Using human stem cells in drug screening can significantly reduce species differences in drug reactions. However, long-term differentiation may increase heterogeneity between organoids and batches, potentially leading to greater diversity in drug evaluations. Multiple omics analyses have revealed the developing heterogeneity of stem cell-derived cells and organoids in 4−5 weeks[42,43]. With spontaneous heterogeneity in cell type and potion, the organoids may not correspond to the pathological tissue and serve to fit in drug screening. Moreover, the induction and maturation of stem cell-derived immune cells remain great challenges in building organoids, which further lingered uncovering of candidates regulating the inflammatory response in MF. Meanwhile, the long duration and high heterogeneity between batches also raised challenges in involving cutting-edge biotechnologies, such as 3D printing to enable drug evaluation in high throughput and multiple dosages[44,45]. This highlights the potential of primary cells as a viable alternative to stem cell induction for achieving phenotypically mature and fully functional cardiomyocyte, fibroblast, or immune cells[46]. In our study, primary cells extracted from rats can fulfill the primary functions of 3 kinds of cells in the 3D hydrogel with defined components and ratios in 3-day screening, demonstrating their potential for widespread use. Considering the tight connection between inflammatory and fibrotic pathways in the pathophysiology[47], BMDMs, the macrophages are involved in the 3D myocardial tissue for improved mimicking of the MF process. Our results emphasized the importance of cellular communication among the three primary cell types in fibrosis through tissue contraction. The significant phenotypic changes in contraction and proliferation suggested great potential for macrophages containing 3D myocardial tissues in candidate screening for inflammatory regulation in the fibrotic process after myocardial injury.

With multiple cell types in the collagen hydrogel, the 3D myocardial tissue could mimic fibrosis and drive tissue contraction under hypoxia, facilitating a rapid and visualized screening of anti-MF candidates. In 3D myocardial tissue, the anti-fibrotic activity of 76 *T. vernicifluum* compounds remained consistent in contraction- and proliferation-based evaluation. However, controversial results of 22 compounds were observed between screening using the traditional 2D−TGF-β−CFs model and 3D myocardial tissue. Among the compounds with controversial activity, only LQ-40 and SQ-3 compounds with anti-fibrosis activity in 3D myocardial tissue showed anti-MF efficacy in the murine LAD model, but not the LQ-39, which was influential in the 2D−TGF-β−CFs model. Although LQ-39, LQ-40, and SQ3 exhibit a similar structural type, the observed discrepancy in biological activity may be attributed to differences in the number of hydroxyl groups on the parent cassettes, differences in the lengths of the side chains leading to different flexibilities, and differences in the number of double bonds. These differences result in different final efficacy outcomes. The mechanism of LQ-40 and SQ-3 may be related to macrophage regulation, as indicated by reduced CD86 signals. This may be because LQ-40 and SQ-3 both have long side chains containing double bonds. After cardiomyocyte injury induced by acute hypoxia-ischemia, large numbers of macrophages are recruited to the site of injury, exert phagocytic and pro-inflammatory effects, clear damaged cardiomyocytes, and subsequently secrete TNF-α, TGF-β, stimulating fibroblast proliferation and producing fibrotic scarring[48]. The high binding potency of LQ-40 and SQ-3 with TSP-1, a matricellular protein that has been reported as a mediator of cardiac fibrosis, required further validations as a target of LQ-40 and SQ-3 in regulating MF[49]. Nevertheless, the upgrade of 2D−TGF-β−CFs to 3D myocardial tissue is recommended in uncovering anti-myocardial fibrosis candidates to reduce both false-positive and false-negative results.

Traditional Chinese medicine and natural plants have shown broad prospects in the treatment of myocardial fibrosis, among which *T. vernicifluum* has a wide range of anti-inflammatory and anti-fibrotic activities, making it an ideal natural compound library for this experimental study. 76 compounds isolated from the resins of *T. vernicifluum* showed anti-fibrosis activities in 3D myocardial tissue under hypoxia, and the main active compounds were urushiols and flavonoids. Interestingly, the compound LQ-40, which was screened and validated in the 3D model and LAD mouse model, belongs to urushiol and is a product of the self-damage repair mechanism of lacquer trees[12]. Many similar natural medicinal plants maintain their health through self-repairing damage mechanisms, including secreting sap, forming callus tissue, repairing damaged areas, and regenerating new tissue to restore normal function[50]. For example, Sanguis Draconis, *Salvia miltiorrhiza*, Radix Notoginseng, etc., impressively, the products secreted due to the self-repairing damage mechanisms generally have the effect of promoting blood circulation and removing blood stasis[51,52], thus having sound therapeutic effects on myocardial fibrosis. Therefore, the results strongly suggest that this type of natural plant with damage repair mechanisms and their products will provide a natural pre-selected drug library for the treatment of myocardial fibrosis.

In summary, this study aims to establish an *in vitro* 3D multicellular model for anti-MF candidate screening. The resulting 3D myocardial tissue will be a reference for related cardiovascular disease research. However, the study is limited by the need for more investigation of crosstalk between three cell types, the mechanism of LQ-40 and SQ-3 in anti-MF, the experimental validation of drug targets, and the involvement of other cell types in MF development. It is essential to explore the mechanism of multicellular response to magnetic fields and to develop a hypothesis for subsequent optimization of 3D cardiac-like tissue.

5. Conclusions

This study established a new 3D myocardial tissue model by integrating primary cardiomyocytes, cardiac fibroblasts, and bone marrow-derived macrophages into collagen hydrogel under hypoxia. It is fully functional, with a defined composition and contractile phenotype, allowing a more sensitive and reliable screening of potential anti-MF drugs compared to the traditional 2D−TGF-β−CFs model. Using this 3D myocardial tissue, two novel candidates derived from the traditional Chinese medicine *T. vernicifluum*, LQ-40, and SQ-3 were discovered and further validated in the murine LAD model. The novel 3D myocardial tissue and the validated anti-MF candidates would inspire further research into cellular crosstalk and new therapies for the treatment of MF.

Acknowledgments

This study was supported by grants from the National Natural Science Foundation of China (Nos. 82222075, 82374420, and

82174215), and Key Research and Development Project of Shandong province (2021CXGC010507, China). We thank Home for Researchers (www.home-for-researchers.com) and Figdraw for polishing Figs. 1 and 8I.

Author contributions

Jingyu Wang: Writing − review & editing, Writing − original draft, Software, Methodology, Formal analysis, Conceptualization. Xiangning Liu: Writing − review & editing, Writing − original draft, Validation, Software, Methodology, Formal analysis, Data curation, Conceptualization. Rongxin Zhu: Software, Data curation. Ying Sun: Software, Methodology. Boyang Jiao: Software, Project administration, Methodology, Investigation. Keyan Wang: Methodology, Formal analysis. Yong Jiang: Project administration, Methodology, Data curation. Yong Wang: Writing − review & editing, Supervision, Funding acquisition. Chun Li: Writing − review & editing, Supervision, Funding acquisition. Wei Wang: Writing − review & editing, Funding acquisition.

Conflicts of interest

The authors declare no competing interests.

Appendix A. Supporting information

Supporting information to this article can be found online at https://doi.org/10.1016/j.apsb.2025.04.025.

References

1. Frangogiannis NG. Cardiac fibrosis. *Cardiovasc Res* 2021;**117**: 1450−88.
2. Martos R, Baugh J, Ledwidge M, O'Loughlin C, Conlon C, Patle A, et al. Diastolic heart failure: evidence of increased myocardial collagen turnover linked to diastolic dysfunction. *Circulation* 2007; **115**:888−95.
3. Ma ZG, Yuan YP, Wu HM, Zhang X, Tang QZ. Cardiac fibrosis: new insights into the pathogenesis. *Int J Biol Sci* 2018;**14**:1645−57.
4. Desroches BR, Zhang P, Choi BR, King ME, Maldonado AE, Li W, et al. Functional scaffold-free 3-D cardiac microtissues: a novel model for the investigation of heart cells. *Am J Physiol Heart Circ Physiol* 2012;**302**:H2031−42.
5. Sadeghi AH, Shin SR, Deddens JC, Fratta G, Mandla S, Yazdi IK, et al. Engineered 3D cardiac fibrotic tissue to study fibrotic remodeling. *Adv Healthc Mater* 2017;**6**:1601434.
6. Meng XM, Nikolic-Paterson DJ, Lan HY. TGF-β: the master regulator of fibrosis. *Nat Rev Nephrol* 2016;**12**:325−38.
7. Peng D, Fu M, Wang M, Wei Y, Wei X. Targeting TGF-β signal transduction for fibrosis and cancer therapy. *Mol Cancer* 2022;**21**:104.
8. Mastikhina O, Moon BU, Williams K, Hatkar R, Gustafson D, Mourad O, et al. Human cardiac fibrosis-on-a-chip model recapitulates disease hallmarks and can serve as a platform for drug testing. *Biomaterials* 2020;**233**:119741.
9. Ingber DE. Reverse engineering human pathophysiology with organs-on-chips. *Cell* 2016;**164**:1105−9.
10. Chen X, Liu S, Han M, Long M, Li T, Hu L, et al. Engineering cardiac tissue for advanced heart-on-a-chip platforms. *Adv Healthc Mater* 2024;**13**:2301338.
11. Revelo XS, Parthiban P, Chen C, Barrow F, Fredrickson G, Wang H, et al. Cardiac resident macrophages prevent fibrosis and stimulate angiogenesis. *Circ Res* 2021;**129**:1086−101.
12. Hu X, Wang M, Cai F, Liu L, Cheng Z, Zhao J, et al. A comprehensive review of medicinal *Toxicodendron* (anacardiaceae): botany, traditional uses, phytochemistry and pharmacology. *J Ethnopharmacol* 2024;**318**:116829.
13. Saravanakumar K, Chelliah R, Hu X, Oh DH, Kathiresan K, Wang MH. Antioxidant, anti-lung cancer, and anti-bacterial activities of *Toxicodendron vernicifluum*. *Biomolecules* 2019;**9**:127.
14. Li W, Du Q, Li X, Zheng X, Lv F, Xi X, et al. Eriodictyol inhibits proliferation, metastasis and induces apoptosis of glioma cells *via* PI3K/Akt/NF-κB signaling pathway. *Front Pharmacol* 2020;**11**:114.
15. Li MC, Zhang YQ, Meng CW, Gao JG, Xie CJ, Liu JY, et al. Traditional uses, phytochemistry, and pharmacology of *toxicodendron vernicifluum* (Stokes) F.S. Barkley—a review. *J Ethnopharmacol* 2021;**267**:113476.
16. Gil MN, Choi DR, Yu KS, Jeong JH, Bak DH, Kim DK, et al. *Rhus verniciflua* Stokes attenuates cholestatic liver cirrhosis-induced interstitial fibrosis *via* Smad3 down-regulation and Smad7 up-regulation. *Anat Cell Biol* 2016;**49**:189−98.
17. Zhang YH, Liu JT, Wen BY, Liu N. Mechanisms of inhibiting proliferation of vascular smooth muscle cells by serum of rats treated with Dahuang Zhechong pill. *J Ethnopharmacol* 2009;**124**:125−9.
18. Ai J, Nie J, He J, Guo Q, Li M, Lei Y, et al. GQ5 hinders renal fibrosis in obstructive nephropathy by selectively inhibiting TGF-β-induced Smad3 phosphorylation. *J Am Soc Nephrol* 2015;**26**:1827−38.
19. Ricard-Blum S. The collagen family. *Cold Spring Harbor Perspect Biol* 2011;**3**:004978.
20. Zhao H, Zhou L, Zhang Q, Zhou X, Zhang Y, Chen H, et al. Bi-content micro-collagen chip provides contractility-based biomechanical readout for phenotypic drug screening with expanded and profiled targets. *Lab Chip* 2015;**15**:3481−94.
21. Cardiff RD, Miller CH, Munn RJ. Manual hematoxylin and eosin staining of mouse tissue sections. *Cold Spring Harb Protoc* 2014;**6**: 655−8.
22. Berman HM, Westbrook J, Feng Z, Gilliland G, Bhat TN, Weissig H, et al. The protein data bank. *Nucleic Acids Res* 2000;**28**:235−42.
23. Eberhardt J, Santos D, Tillack AF, Forli S. AutoDock Vina 1.2.0: new docking methods, expanded force field, and python bindings. *J Chem Inf Model* 2021;**61**:3891−8.
24. Nicks AM, Holman SR, Chan AY, Tsang M, Young PE, Humphreys DT, et al. Standardised method for cardiomyocyte isolation and purification from individual murine neonatal, infant, and adult hearts. *J Mol Cell Cardiol* 2022;**170**:47−59.
25. Rutering J, Ilmer M, Recio A, Coleman M, Vykoukal J, Alt E. Improved method for isolation of neonatal rat cardiomyocytes with increased yield of c-Kit$^+$ cardiac progenitor cells. *J Stem Cell Res Ther* 2015;**5**:1−8.
26. Lu X, Yao J, Li C, Cui L, Liu Y, Liu X, et al. Shexiang tongxin dropping pills promote macrophage polarization-induced angiogenesis against coronary microvascular dysfunction *via* PI3K/Akt/mTORC1 pathway. *Front Pharmacol* 2022;**13**:840521.
27. Sjöblom B, Salmazo A, Djinović K. Alpha-actinin structure and regulation. *Cell Mol Life Sci* 2008;**65**:2688−701.
28. Ridge KM, Eriksson JE, Pekny M, Goldman RD. Roles of vimentin in health and disease. *Genes Dev* 2022;**36**:391−407.
29. Xiang X, Wang J, Lu D, Xu X. Targeting tumor-associated macrophages to synergize tumor immunotherapy. *Signal Transduct Target Ther* 2021;**6**:75.
30. Litviňuková M, Talavera C, Maatz H, Reichart D, Worth CL, Lindberg EL, et al. Cells of the adult human heart. *Nature* 2020;**588**: 466−72.
31. Pinto AR, Ilinykh A, Ivey MJ, Kuwabara JT, D'Antoni ML, Debuque R, et al. Revisiting cardiac cellular composition. *Circ Res* 2016;**118**:400−9.
32. Gauthier T, Yao C, Dowdy T, Jin W, Lim YJ, Patiño LC, et al. TGF-β uncouples glycolysis and inflammation in macrophages and controls survival during sepsis. *Sci Signal* 2023;**16**:eade0385.
33. Wagstaff AJ, Davis R, McTavish D. Fosinopril: a reappraisal of its pharmacology and therapeutic efficacy in essential hypertension. *Drugs* 1996;**51**:777−91.

34. Kweon YO, Goodman ZD, Dienstag JL, Schiff ER, Brown NA, Burchardt E, et al. Decreasing fibrogenesis: an immunohistochemical study of paired liver biopsies following lamivudine therapy for chronic hepatitis B. *J Hepatol* 2001;**35**:749−55.
35. Rubiś P, Holcman K, Dziewięcka E, Wiśniowska S, Karabinowska A, Szymonowicz M, et al. Relationships between circulating galectin-3, extracellular matrix fibrosis and outcomes in dilated cardiomyopathy. *Adv Clin Exp Med* 2021;**30**:245−53.
36. Julovi SM, Trinh K, Robertson H, Xu C, Minhas N, Viswanathan S, et al. Thrombospondin-1 drives cardiac remodeling in chronic kidney disease. *JACC Basic Transl Sci* 2024;**9**:607−27.
37. Shen P, Jia Y, Zhou W, Zheng W, Wu Y, Qu S, et al. A biomimetic liver cancer on-a-chip reveals a critical role of LIPOCALIN-2 in promoting hepatocellular carcinoma progression. *Acta Pharm Sin B* 2023;**13**:4621−37.
38. Hofbauer P, Jahnel SM, Papai N, Giesshammer M, Deyett A, Schmidt C, et al. Cardioids reveal self-organizing principles of human cardiogenesis. *Cell* 2021;**184**:3299−317.
39. Richards DJ, Li Y, Kerr CM, Yao J, Beeson GC, Coyle RC, et al. Human cardiac organoids for the modelling of myocardial infarction and drug cardiotoxicity. *Nat Biomed Eng* 2020;**4**:446−62.
40. Romeo SG, Secco I, Schneider E, Reumiller CM, Santos CXC, Zoccarato A, et al. Human blood vessel organoids reveal a critical role for CTGF in maintaining microvascular integrity. *Nat Commun* 2023; **14**:5552.
41. Gao Z, Du Z, Hou Y, Hua K, Tu P, Ai X, et al. A microfluidic coculture model for mapping signaling perturbations and precise drug screening against macrophage-mediated dynamic myocardial injury. *Acta Pharm Sin B* 2024;**14**:5393−406.
42. Fernandes I, Funakoshi S, Hamidzada H, Epelman S, Keller G. Modeling cardiac fibroblast heterogeneity from human pluripotent stem cell-derived epicardial cells. *Nat Commun* 2023;**14**:8183.
43. Lassé M, El Saghir J, Berthier CC, Eddy S, Fischer M, Laufer SD, et al. An integrated organoid omics map extends modeling potential of kidney disease. *Nat Commun* 2023;**14**:4903.
44. Grebenyuk S, Abdel Fattah AR, Kumar M, Toprakhisar B, Rustandi G, Vananroye A, et al. Large-scale perfused tissues *via* synthetic 3D soft microfluidics. *Nat Commun* 2023;**14**:193.
45. Ong CS, Fukunishi T, Zhang H, Huang CY, Nashed A, Blazeski A, et al. Biomaterial-free three-dimensional bioprinting of cardiac tissue using human induced pluripotent stem cell derived cardiomyocytes. *Sci Rep* 2017;**7**:4566.
46. Wang Y, Gao Y, Pan Y, Zhou D, Liu Y, Yin Y, et al. Emerging trends in organ-on-a-chip systems for drug screening. *Acta Pharm Sin B* 2023; **13**:2483−509.
47. Wynn TA, Vannella KM. Macrophages in tissue repair, regeneration, and fibrosis. *Immunity* 2016;**44**:450−62.
48. Swirski FK, Nahrendorf M. Cardioimmunology: the immune system in cardiac homeostasis and disease. *Nat Rev Immunol* 2018;**18**: 733−44.
49. Murphy-Ullrich JE, Suto MJ. Thrombospondin-1 regulation of latent TGF-β activation: a therapeutic target for fibrotic disease. *Matrix Biol* 2018;**68**−**69**:28−43.
50. Xu C, Cao H, Zhang Q, Wang H, Xin W, Xu E, et al. Control of auxin-induced callus formation by bZIP59−LBD complex in arabidopsis regeneration. *Nat Plants* 2018;**4**:108−15.
51. Tao H, Yang X, Wang W, Yue S, Pu Z, Huang Y, et al. Regulation of serum lipidomics and amino acid profiles of rats with acute myocardial ischemia by *Salvia miltiorrhiza* and *Panax notoginseng* herb pair. *Phytomedicine* 2020;**67**:153162.
52. Li C, Zhang Y, Wang Q, Meng H, Zhang Q, Wu Y, et al. Dragon's blood exerts cardio-protection against myocardial injury through PI3K−AKT−mTOR signaling pathway in acute myocardial infarction mice model. *J Ethnopharmacol* 2018;**227**:279−89.